Available online at www.sciencedirect.com
SCIENCE DIRECT®
PERGAMON
International Journal of Heat and Mass Transfer 46 (2003) 2471–2483
International Journal of HEAT and MASS TRANSFER
www.elsevier.com/locate/ijhmt

Analysis of convective momentum and wall heat transfer: application to vortex boundary layer interaction

Xavier Escriva [a], André Giovannini [b,*]

[a] CERFACS, 42, Avenue Gaspard Coriolis, 31057 Toulouse Cedex 1, France
[b] Université Paul Sabatier, Institut de Mécanique des Fluides de Toulouse, UMR 5502 CNRS/INP/UPS, 118, Route de Narbonne, 31062 Toulouse Cedex, France

Received 28 May 2002

Abstract

The main topic of this paper is the analysis of momentum and heat transfer mechanisms occurring inside a disturbed boundary layer. This analysis is carried out based on a phenomenological decomposition using von Karman's integral equations, in which appear terms that account for several contributions: the flat plate term, and the unsteady and external gradient terms.

This method is applied to the interaction between a single transverse vortex and a boundary layer developing on a flat plate. Based on numerical simulations, we present a qualitative and quantitative study of the behavior of momentum and heat wall transfer described by the terms resulting from the phenomenological decomposition. Finally, the time-dependent behavior of the analogy factor is investigated.

Keywords: Wall transfer; Skin friction; Heat flux; Vortex boundary layer interaction; Analogy factor

1. Introduction

In many investigations involving convective heat transfer in the proximity of a solid wall, the analogy between dynamic and thermal fields as transfer coefficients is often claimed. This analogy defined in various books [1,2], derived from the similarities between momentum and heat equations with their related boundary conditions, is valid only for a flow along a flat plate with uniform boundary conditions.

Nevertheless, it appears that either instantaneous or time averaged, this analogy is very often used far from the original domain of validity. As examples, we refer to heat enhancement techniques with riblets, optimisation of heat transfer in heat exchangers circuits, electronic circuits, heat sinks and heavy-duty devices embedded in turbine blades of aeronautical engines. In those situations featuring particularly ribbed walls or impacting jets, we are far from the mathematical models in which the analogy remains valid.

Another field of interest for the vortex boundary layer interaction is the modelisation of the turbulent boundary layer with thermal effects. Indeed, vortex structures inside the outer layer affect the thin viscous layer in ways similar to the way which the vortex interacts with the boundary layer. Although various dynamic models exist, the thermal modeling usually relies on algebraic models such as the turbulent Prandtl model.

In the present work, we put forward our analysis based on the decomposition term by term of the von Karman's integral equations for momentum and heat transfer. The first objective is the understanding of physical response of boundary layers in situations far more complex than the so-called "flat plate uniform situation". This is achieved thanks to well-known solutions of the unsteady dynamic and thermal von Karman

* Corresponding author. Tel.: +33-5-6128-5948; fax: +33-5-6128-5992.
E-mail address: andre.giovannini@imft.fr (A. Giovannini).

0017-9310/03/$ - see front matter
doi:10.1016/S0017-9310(02)00547-1

Nomenclature

Normal characters

C_p	specific heat at constant pressure ($J\,kg^{-1}\,K^{-1}$)
p	static pressure ($kg\,m\,s^{-2}$)
$\mathbf{u}$	velocity vector ($m\,s^{-1}$)
u, v	instantaneous components of velocity ($m\,s^{-1}$)
U_∞	freestream velocity ($m\,s^{-1}$)
t	time variable (s)
T_∞	freestream temperature ($m\,s^{-1}$)
T_w	wall temperature (K)
x, y	longitudinal and transverse coordinates (m)

Greek characters

Γ	vortex circulation ($m^2\,s^{-1}$)
γ	dimensionless circulation
δ, Δ	dynamic and thermal boundary layer thicknesses (m)
δ_1, Δ_1	dynamic and thermal displacement boundary layer thicknesses (m)
δ_2, Δ_2	momentum and enthalpy boundary layer thicknesses (m)
δ_3	kinetic energy boundary layer thickness (m)
μ	dynamic viscosity coefficient ($kg\,m^{-1}\,s^{-1}$)
ν	kinematic viscosity coefficient ($m^2\,s^{-1}$)
ρ	fluid density ($kg\,m^{-3}$)
τ_w	wall shear stress ($kg\,m^{-1}\,s^{-2}$)
φ_w	wall heat flux ($W\,m^{-2}$)
$\boldsymbol{\omega}$	vorticity vector (s^{-1})
ω_z	transverse vorticity components (s^{-1})

Dimensionless numbers

Cf	skin friction coefficient
Ch	heat transfer coefficient (or Stanton number)
Cp	wall pressure coefficient
Ek	Eckert number
M	Mach number
Pr	Prandtl number
Re	Reynolds number
Re_Γ	vortex circulation based Reynolds number
s	analogy factor $\left(=\frac{2Ch}{Cf}\right)$

Subscripts

∞	related to freestream
w	related to wall
t, Γ	related to the vortex
fp	related to flat plate term
unst	related to unsteady term
ext	related to external gradient term

integral equations. The first part of this paper (Sections 2–4) is devoted to this phenomenological analysis with elementary boundary layer solutions.

In Section 5, our second objective is to simulate the interaction of a single vortex with a laminar boundary layer. With the same phenomenological decomposition used in the first part, we will provide a local analysis of the dynamic and thermal transfer coefficients and the analogy factor when the boundary layer is affected by the unsteady field velocity of the vortex.

Previous works related to the vortex boundary interaction are mostly numerical simulations and very few take in account thermal effects. The first reference to vortex boundary interaction is due to Harvey and Perry [3] where the motivation of this study lays in the decay of wing tip vortices near airport runways. Doligalski and Walker [4] gave theoretical backgrounds and asymptotical solutions of the interaction. Experimental characterisation and studies of the interaction were carried out by Peube and Ferret [5] and Reulet [6]: the first paper is dealing with vortex generation and fluid mechanics aspects whereas in the second one, some of the results obtained are quite confusing as the wake vortex due to the generator triggers the turbulence in the boundary layer flow on the plate downstream. Corjon and Poinsot [7] provided numerical simulations of the interaction of two counter-rotating vortices with a boundary layer, modelling the wing tip vortices problem as depicted by Harvey et al. Pellerin [8] studied a single vortex interaction with a boundary layer but without thermal effects. Finally, Tafti [9] carried throughout a dynamic and thermal analysis, however the periodic vortex shedding generated with a thin vertical plate upstream the boundary layer prevent the author from a clear statement about the behavior of the dynamic and thermal transfer coefficients during the interaction. So it appears that the literature devoted to both dynamic and thermal behaviour is very sparse and not clear in the conclusions.

With the simulation of the vortex boundary layer interaction, we expect to establish some links between the theoretical approach used in the first part and more physical and industrial applications like those depicted previously (heat transfer enhancement, turbulent boundary layer models).

2. Mathematical formulation of the boundary layer

In this part we write the governing equations of the boundary layer with the following three assumptions, which won't reduce the scope of our analysis.

The physical model involves a Newtonian fluid with flows in a range from moderate up to large Reynolds numbers. The hypotheses $\mathscr{H}_1$ and $\mathscr{H}_2$ for the flow and heat transfer are respectively the incompressibility (Mach number $M \ll 1$) and non-dilatability for the fluid. The second assumption reads:

$$\frac{T_w - T_\infty}{T_\infty} \ll 1 \tag{1}$$

Upon these two assumptions, the flow is driven by isovolume evolution.

We define the Eckert number as:

$$Ek = \frac{U_\infty^2}{C_p(T_\infty - T_w)} \approx \frac{M^2}{\frac{T_w - T_\infty}{T_\infty}} \tag{2}$$

Thus if we want to neglect the volumetric power terms associated with pressure works and viscous dissipation with respect to the other terms, we should add hypothesis $\mathscr{H}_3$ ($Ek = 0$) for sake of regularity (well posedness) of the ratio between kinematic heating and thermal heating.

In the following, we will restrict ourselves to a heated flat plate boundary layer flow. The equations are scaled using U_∞, ρU_∞^2 and $T_\infty - T_w$ quantities respectively for the velocity, pressure and temperature difference $T - T_w$. The resulting mathematical model reads as follows:

$$\frac{\partial \bar{u}}{\partial \bar{t}} + \bar{u}\frac{\partial \bar{u}}{\partial \bar{x}} + \bar{v}\frac{\partial \bar{u}}{\partial \bar{y}} = -\frac{\partial \bar{p}}{\partial \bar{x}} + \frac{1}{Re}\frac{\partial^2 \bar{u}}{\partial \bar{y}^2} \tag{3}$$

$$\frac{\partial \overline{T}}{\partial \bar{t}} + \bar{u}\frac{\partial \overline{T}}{\partial \bar{x}} + \bar{v}\frac{\partial \overline{T}}{\partial \bar{y}} = \frac{1}{RePr}\frac{\partial^2 \overline{T}}{\partial \bar{y}^2} \tag{4}$$

with dimensionless variables:

$$\bar{u} = \frac{u}{U_\infty} \quad \bar{v} = \frac{v}{U_\infty} \quad \overline{T} = \frac{T - T_w}{T_\infty - T_w} \quad \bar{p} = \frac{p}{\rho U_\infty^2}$$

The associated boundary conditions are: $\bar{u} = \overline{T} = 0$ at the wall and $\bar{u} = \overline{T} = 1$ in the free stream flow.

As general observations, we make the two following statements. First, we notice that dynamic and thermal equations differ one another from the longitudinal pressure gradient term and the diffusion coefficients. Thus, introducing the velocity-vorticity formulation, the mathematical analogy between the transverse component of the vorticity ω_z and the temperature is obvious:

$$\frac{\partial \bar{\omega}_z}{\partial \bar{t}} + \bar{u}\frac{\partial \bar{\omega}_z}{\partial \bar{x}} + \bar{v}\frac{\partial \bar{\omega}_z}{\partial \bar{y}} = \frac{1}{Re}\frac{\partial^2 \bar{\omega}_z}{\partial \bar{y}^2} \tag{5}$$

However boundary conditions at the wall remains different due to the implicit boundary condition for the vorticity ω_z at the wall.

Now, back to the original set of equations (3) and (4), we give some definitions. First, we notice that the analogy is fulfilled when the pressure gradient is zero and the Prandtl number is equal to one. This is known as the Reynolds analogy, for laminar and turbulent flow (with algebraic models). The main consequence is the equality between dimensionless velocity and temperature profiles: $\bar{u} = \overline{T}$. In this case, the analogy factor is equal to unity and defined as follows:

$$s = \frac{2Ch}{Cf} = 1$$

where:

$$\frac{Cf}{2} = \frac{\vec{e}_x \cdot \vec{\sigma}_v \cdot \vec{e}_y|_w}{\rho_\infty U_\infty^2} = \frac{\tau_w}{\rho_\infty U_\infty^2} = \frac{1}{Re}\left.\frac{\partial \bar{u}}{\partial \bar{y}}\right|_w = -\frac{\bar{\omega}_z|_w}{Re} \tag{6}$$

$$Ch = \frac{\vec{q} \cdot \vec{e}_y|_w}{\rho_\infty U_\infty C_p(T_w - T_\infty)} = \frac{\varphi_w}{\rho_\infty U_\infty C_p(T_w - T_\infty)} = \frac{1}{RePr}\left.\frac{\partial \overline{T}}{\partial \bar{y}}\right|_w \tag{7}$$

However, in most cases, convective, diffusive and acoustic time scales encountered in Eqs. (3) and (4) have very different orders of magnitude, and full mathematical models are required to take into account all physicals effects as the pressure gradient, the Prandtl number and the boundary condition effects (e.g.: blowing throughout the wall or time dependent free stream velocity or/and temperature).

The next sections are organized as follows. First, we reconsider the dynamic and thermal von Karman equations in a more general context. Each term in these equations will be defined and identified respectively as the *flat plate term* (related to undisturbed steady boundary layer flow), the *unsteady term* (related to unsteady boundary layer flow) and the *external gradient term* (related to free stream dependent perturbations). Parametric sensitivity to Prandtl number is investigated in Section 4.

In Section 5, we investigate by numerical simulation the interaction of a transverse vortex with a boundary layer using the above-mentioned phenomenological decomposition. Although this flow is rather academic, it is nevertheless found in unsteady separating flows like boundary layers flow with obstacles like ribbed walls or vortex blades interaction in turbine stage of aeronautical engines.

3. Dynamic and thermal von Karman equations

Following von Karman method, we integrate Eqs. (3) and (4) along the normal direction from the wall to infinity. It results in a tangential wall shear stress τ_w term and wall heat flux φ_w term as functions of dynamic boundary layer thicknesses (δ_i, $i = \{1, 2, 3\}$) and thermal boundary layer thicknesses (Δ_i, $i = \{1, 2\}$) which definitions are to be found in [10].

3.1. Unsteady dynamic von Karman equation

We extend the usual von Karman equation with hypothesis $\mathscr{H}_1$ and $\mathscr{H}_2$ to unsteady boundary layer situations. Those equations reads as follows:

$$\frac{\tau_w}{\rho_\infty} = \frac{\partial}{\partial t}(U_\infty \delta_1) + \frac{\partial}{\partial x}(U_\infty^2 \delta_2) + U_\infty \frac{\partial U_\infty}{\partial x}\delta_1 \tag{8}$$

in which the first term in the right hand side correspond to time dependency.

3.2. Unsteady thermal von Karman equation

The unsteady von Karman thermal equation (with additional hypothesis $\mathscr{H}_3$) obtained using the same procedure as for steady case is less usual. The wall heat flux is expressed as follows:

$$\frac{\varphi_w}{\rho_\infty} = \frac{\partial}{\partial t}[C_p \Delta_1 (T_w - T_\infty)] + \frac{\partial}{\partial x}[C_p (T_w - T_\infty) U_\infty \Delta_2] - U_\infty \delta_1 \left[C_p \frac{\partial T_\infty}{\partial x} + U_\infty \frac{\partial U_\infty}{\partial x} \right] \tag{9}$$

From Eqs. (8) and (9), we propose a obvious decomposition of each term in Table 1. We classify each term according to their physical meaning as we suggested in the previous section: the unsteady term, the flat plate term and the external gradient term. If hypothesis $\mathscr{H}_3$ is not retained, additional terms shown in the third column of Table 1 are to be considered.

This is a phenomenological decomposition or splitting of the unsteady von Karman equation, because each of these terms could be related with simple solutions in which this physical behavior is dominant. Therefore Prandtl number influence for each term of the von Karman equation can be study through analytical or accurate numerical solutions of the corresponding academical cases.

At this step, the analogy between dynamic and thermal terms (with the outstanding exception of the external gradient terms) is straightforward if we substitute U_∞ by $(T_w - T_\infty)$ and dynamic boundary layer thicknesses by the thermal ones. We will precise further this aspect in the following paragraph.

4. Analysis term by term of the phenomenological decomposition

In this section, we give a full set of solutions for each terms involved in the decomposition using some results from the literature.

4.1. The flat plate term

The physical flow related to this term is a heated flat plate without external perturbations. Since Blasius and Polhausen stepping stone works, the solution of this problem is well known and obtained by a transformation of the partial derivatives momentum equation (Eq. (3)) into a third order nonlinear ordinary derivatives equation.

For dynamic solution, we refer to [11,12] for the classical Blasius equation and variable definition.

For the thermal solution, the same procedure is applied to the general thermal equation (with kinetic heating effects) which is a quasi-linear second order ODE:

$$\theta''(\eta) + \frac{Pr}{2} f(\eta)\theta(\eta) + Pr\,Ek\, f''^2 = 0 \tag{10}$$

with associated boundary conditions:

$$\theta(0) = 0 \quad \text{and} \quad \theta(\infty) = 1$$

The resulting expression for $\theta(\eta)$ follows:

$$\theta(\eta) = 1 - \left(1 - \frac{\int_0^\eta f''^{Pr}\,d\eta'}{\int_0^\infty f''^{Pr}\,d\eta}\right)\left(1 + \xi(0)\frac{Ek}{2}\right) + \xi(\eta)\frac{Ek}{2}$$
$$\text{with } \xi(\eta) = 2Pr \int_\eta^\infty f''^{Pr}\left(\int_0^{\eta'} f''^{2-Pr}\,d\eta''\right)d\eta' \tag{11}$$

By computing boundary layer thicknesses and wall coefficients (skin friction and heat transfer), we get the value of the analogy factor as a function of the Prandtl number:

$$s_{fp} = \frac{\theta'(0)}{f''(0)Pr} = \frac{1}{Pr}\left(\frac{f''^{Pr-1}(0)}{\int_0^\infty f''^{Pr}\,d\eta}\right)\left(1 + \frac{Ek}{2Pr}\xi(0)\right) \tag{12}$$

Table 1
Von Karman term decomposition classification

Term	τ_w/ρ_∞	$\varphi_w/(\rho_\infty C_p)$	Term Ek ($Ek \neq 0$)
Flat plate	$U_\infty^2 \frac{\partial \delta_2}{\partial x}$	$U_\infty (T_w - T_\infty)\frac{\partial \Delta_2}{\partial x}$	$\frac{Ek}{2}\frac{\partial \delta_3}{\partial x}$
Unsteady	$\frac{\partial}{\partial t}(U_\infty \delta_1)$	$\frac{\partial}{\partial t}[(T_w - T_\infty)\Delta_1]$	$\frac{Ek}{2}(\delta_1 + \delta_2)$
External gradient	$U_\infty \frac{\partial U_\infty}{\partial x}(\delta_1 + 2\delta_2)$	$\frac{\partial}{\partial x}[U_\infty (T_w - T_\infty)]\Delta_2 - U_\infty \frac{\partial T_\infty}{\partial x}\delta_1$	$\frac{Ek}{2}(2\delta_1 + \delta_3)$

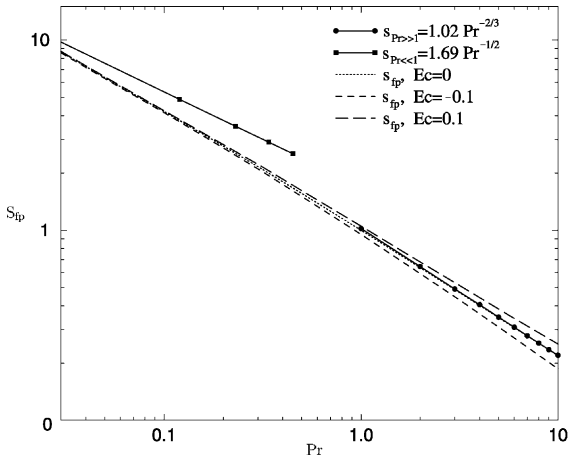

Fig. 1. Analogy factor on a flat plate: $s_{\mathrm{fp}}(Pr, Ek)$ (log–log graph).

We report in Fig. 1, the variation of s_{fp} against Prandtl number for three values of Ek. The evolution for $Ek = 0$ is to be compared with the asymptotic laws for $Pr \gg 1$ and $Pr \ll 1$ referred by Bejan [11]. Values of the analogy factor below $Pr = 0.05$ are hardly reliable, because of roundoff errors polluting the numerical integration of the former equation.

Using the analogy factor s_{fp} definition and the expression of the wall sheet stress and wall heat flux, we obtain the analogy factor as function of the boundary layer thicknesses:

$$s_{\mathrm{fp}} = \frac{\Delta_2}{\delta_2} + \frac{Ek}{2}\frac{\delta_3}{\delta_2} = f_{\mathrm{fp}}(Pr, Ek) + 1.57\frac{Ek}{2} \tag{13}$$

First, we note that $f_{\mathrm{fp}}(Pr, Ek) = f_{\mathrm{fp}}(Pr) \backsimeq Pr^{-2/3}$ for low Eckert numbers which is a well-known result mentioned by Kays and Crawford [1]. Then, we notice that momentum and enthalpy thicknesses are analogous i.e. their variations scale with a multiplicative constant.

4.2. The unsteady term

Here, we assume the flow and heat transfer are invariant with the longitudinal direction (stream lines and temperature isolines are parallel to the horizontal solid flat plate). This problem is well documented in the literature and referred as Rayleigh–Stokes problem. The corresponding set of equations (see [12]) is:

$$\frac{\partial \bar{u}}{\partial \bar{t}} = \frac{1}{Re}\frac{\partial^2 \bar{u}}{\partial \bar{y}^2} \tag{14}$$

$$\frac{\partial \overline{T}}{\partial \bar{t}} = \frac{1}{RePr}\frac{\partial^2 \overline{T}}{\partial \bar{y}^2} + \frac{1}{Re}\left(\frac{\partial \bar{u}}{\partial \bar{y}}\right)^2 \tag{15}$$

By means of the change of coordinate:

$$\eta = \frac{\bar{y}}{2\sqrt{\nu \bar{t}}}$$

and introducing:

$$f = \frac{\bar{u}}{U_\infty}$$

we reduce the PDE (14) to a linear second order ODE:

$$f'' + 2\eta f' = 0 \tag{16}$$

with boundary conditions: $f(0) = 0$ and $f(\infty) = 1$. The solution is the error function:

$$f(\eta) = \mathrm{erf}(\eta) = \int_0^\eta \mathrm{e}^{-\eta^2}\,\mathrm{d}\eta$$

The dynamic von Karman equation restricted to this term is written as follows:

$$\tau_{\mathrm{w}} = \rho U_\infty \frac{\partial \delta_1}{\partial t} = \rho U_\infty \sqrt{\frac{\nu}{\pi t}} \tag{17}$$

For the thermal problem, solutions for all Prandtl numbers and Eckert numbers can be integrated without a loss of generality. They were computed by integrating of the following ODE:

$$\theta'' + 2Pr\,\eta\theta + Pr\,Ek\,f'^2 = 0 \tag{18}$$

resulting from the change of variable:

$$\theta = \frac{T - T_{\mathrm{w}}}{T_\infty - T_{\mathrm{w}}}$$

As example, we give formal expression in the range $0 < Pr < 2$ (for the whole set of solution, see [13]):

$$\begin{aligned}\theta(\eta)|_{0<Pr<2} = {} & \mathrm{erf}(\eta\sqrt{Pr}) \\ & \times \left[1 + \frac{2Ek}{\pi}\sqrt{\frac{Pr}{2-Pr}}\arctan\left(\sqrt{\frac{2-Pr}{Pr}}\right)\right. \\ & \left. - \mathrm{erf}(\eta\sqrt{2-Pr})\right] \\ & + 2Ek\sqrt{\frac{Pr}{\pi}}\int_0^\eta \mathrm{e}^{-(2-Pr)z^2}\mathrm{erf}(\sqrt{Pr}z)\,\mathrm{d}z\end{aligned} \tag{19}$$

The resulting analogy factor for the same range of Prandtl number values is:

$$s_{\mathrm{unst}} = \frac{\left[1 + \frac{2Ek}{\pi}\sqrt{\frac{Pr}{2-Pr}}\arctan\left(\sqrt{\frac{2-Pr}{Pr}}\right)\right]}{\sqrt{Pr}} \tag{20}$$

and expressed as function of the boundary layer thicknesses:

$$s_{\mathrm{unst}} = \frac{\Delta_1}{\delta_1} + \frac{Ek}{2}\left(1 + \frac{\delta_2}{\delta_1}\right) = f_2(Pr, Ek) + \frac{\sqrt{2}}{2}Ek \tag{21}$$

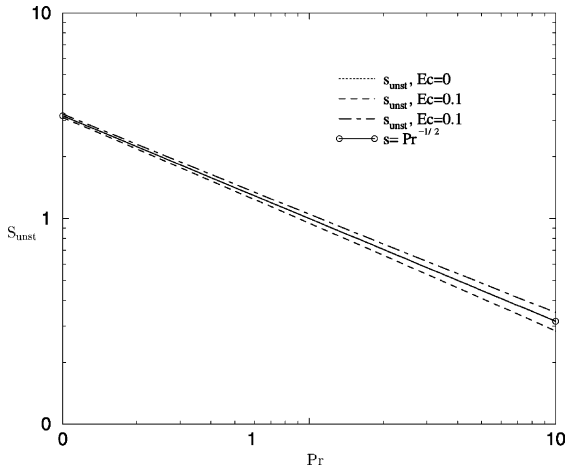

Fig. 2. Unsteady analogy factor: $s_{\text{unst}}(Pr, Ek)$ (log–log graph).

with $f_2(Ek, Pr) = f_2(Pr) = Pr^{-1/2}$ for low Eckert numbers. The evolution of the analogy factor with the Prandtl number ranging from 0 to 10 are reported in Fig. 2 and for three values of Eckert number. We observe that the dynamic and thermal boundary layer displacement thicknesses are analogous.

4.3. External gradient term

In this section, we refer to the Falkner–Skan [14] results about pressure gradient driven boundary layer flow. It is assumed that the free stream velocity U_∞ and temperature $(T_\infty - T_w)$ behave like power law with respect to x:

$$U_\infty(x) = kx^m \quad (T_\infty - T_w)(x) = \lambda x^n$$

$$\text{with } m = \frac{-x}{\rho U_\infty^2}\frac{\mathrm{d}p}{\mathrm{d}x}$$

For the momentum equation, using the same change of variable and function from the Blasius theory, we obtain:

$$f''' + \frac{m+1}{2} f f'' + m(1 - f'^2) = 0 \tag{22}$$

with the following boundary conditions: $f(0) = f'(0) = 0$ and $f'(\infty) = 1$. We get the boundary layer thicknesses and skin friction coefficient by integration of Eq. (22):

$$\delta_1 \sqrt{\frac{U_\infty}{\nu x}} = \int_0^\infty (1 - f')\,\mathrm{d}\eta = [\eta - f]_\infty \tag{23}$$

$$\delta_2 \sqrt{\frac{U_\infty}{\nu x}} = \int_0^\infty f'(1 - f')\,\mathrm{d}\eta = \left[\frac{2}{3m+1} f''(0) - \frac{2m}{3m+1}(\eta - f)_\infty\right] \tag{24}$$

$$\frac{Cf}{2}\sqrt{\frac{U_\infty}{\nu x}} = f''(0) \tag{25}$$

For the thermal equation, self-similar solutions can be found for Eckert number equal to -2 or in the trivial form of the energy equation (stagnation temperature $= T_w$ and $Pr = 1$). These cases apart, the generic equation is:

$$\theta'' + \frac{m+1}{2} Pr f \theta + Pr Ek f''^2 = 0 \tag{26}$$

with boundary conditions: $\theta(0) = 0$ and $\theta(\infty) = 1$. The integration was carried out only for the case $Ek = 0$, the wall heat transfer coefficient expression as function of the Prandtl number and dimensionless pressure gradient m is the following:

$$Ch\,Pr\sqrt{\frac{U_\infty}{\nu x}} = \theta'(0) = \frac{1}{\int_0^\infty \exp(-Pr\frac{m+1}{2}\int_0^{\eta'} f\,\mathrm{d}\eta')\,\mathrm{d}\eta} \tag{27}$$

In Fig. 3, we report variations of skin friction coefficient Cf and heat transfer coefficient Ch as function of the dimensionless pressure gradient m within a range from $m = -0.0904$ to 1 and three values of the Prandtl number. The skin friction coefficient curve grows faster than the heat transfer coefficient curve within the range of medium to high Prandtl number. Near the separation flow conditions where dimensionless pressure gradient value m equals -0.0904, Cf curve tends to zero whereas Ch curves values remains strictly positive even for high Prandtl numbers.

In Fig. 4, we plotted the analogy factor s_{ext} as function of the dimensionless pressure gradient m. We make the following remarks with respect to the role of pressure gradient on the analogy factor:

Limiting the range of analysis from the lower bound $m = -0.0904$ (separation) to the upper bound $m = 1$ (stagnation flow), we denote in particular the unsymmetrical behavior of the analogy factor around the mean zero value of the gradient ($m = 0$, flat plate flow without

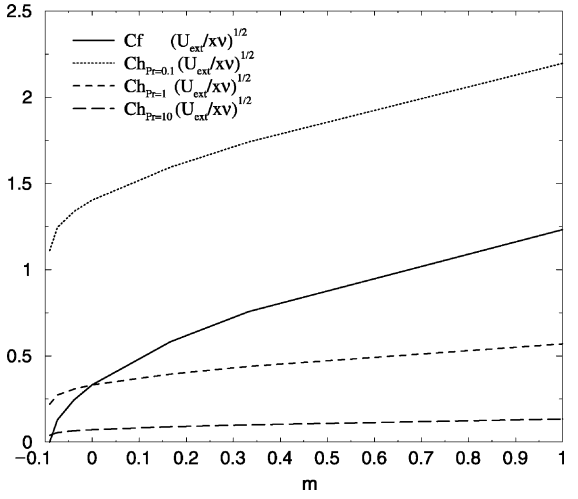

Fig. 3. Skin friction coefficient and heat transfer coefficient as function of m and Prandtl number.

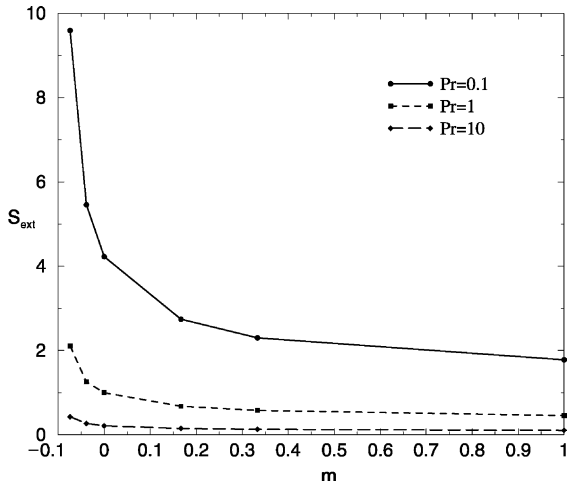

Fig. 4. Analogy factor as function of m for three values of Prandtl number.

gradient). This is a worthy result: Indeed, if we consider successively negative and positive pressure gradient variation during a vortex sweeping above the wall, the mean value of the time integrated analogy factor will be greater than the value for $m = 0$.

The second interesting behavior is related with the analogy breaking between dynamic and thermal boundary layers thicknesses behaviour. Indeed, if we look at the particular case $m = 1$, the expression of the analogy factor simplifies drastically as the boundary layer thicknesses become constant:

$$s_{\text{ext}}(m=1) = \frac{\Delta_2}{\delta_1 + 2\delta_2} + \frac{Ek}{2}\left(\frac{3\delta_3 - 2\Delta_2}{\delta_1 + 2\delta - 2}\right) \tag{28}$$

Therefore even for low Eckert numbers, dynamic and thermal wall transfer are no longer analogous in the classic sense, because enthalpy thickness Δ_2 scales with the linear combination of the dynamic thicknesses δ_1 and δ_2.

However for low Eckert number, the analogy factor for pressure gradient driven boundary layer flow, may be reduced to a non-linear function of m: $f_{\text{NL}}(m)$ and a power law function of Prandtl number:

$$s_{\text{ext}}(m, Pr) = f_{\text{NL}}(m) Pr^{-2/3} \tag{29}$$

with a singularity ($s_{\text{ext}}(m, Pr) \to \infty$) when $m \to -0.0904$ [13].

5. Application to the vortex boundary layer interaction

5.1. Problem outline

Our main objective in this section is to study numerically the interaction of a transverse vortex structure with a laminar heated boundary layer over a flat plate and therefore extract simple dynamic and thermal behaviors of the interaction throughout the phenomenological decomposition. The finite volume code used, CUTEFLOWS, allows us to simulate the flow but also to post-treat the results thanks to the phenomenological decomposition methodology described earlier and implemented in the code.

We expose the methodology and give an example of interaction simulated for a given strength of interaction. We simulate a Navier–Stokes incompressible flow with low dilatability and very small Eckert number ($Ek \approx 10^{-3}$).

The numerical model handles the spatial discretization through second order finite volume methods and second order Runge–Kutta scheme for time stepping. The code gathering these techniques named CUTEFLOWS [15] has been validated over a wide number of cases in the literature. We report a few examples for cartesian geometries: Treidler [16] used it for flows in ribbed channels, Giovannini and Bortolus [17,18] simulated a turbulent flow past a backward step. For cylindrical geometries Suzuki and Humphrey [19] studied flows between corotating disks in fixed enclosures and finally Dainese [20] simulated a tri-dimensional flow in a helicoidal duct.

The non-uniform cartesian mesh is structured with a averaged density of 315 nodes by meter in the longitudinal direction and 1080 nodes by meter in the transversal direction with increasing density close to the boundary layer. The geometry and boundary conditions are sketched in Fig. 5.

The Reynolds number at the end of the plate is $Re_L = 1.1 \times 10^5$ and the vortex Reynolds number defined as:

$$Re_\Gamma = \frac{\Gamma}{2\pi\nu}$$

is equal to 2032. The Prandtl number is equal to air Prandtl value at 300 K ($Pr = 0.7$). Reference length scales are the viscous radius core ($r_o = 0.02$ m) for the vortex, the boundary thickness at the end of the plate ($\delta_L = 0.0134$ m) for the boundary layer and for the interaction the vortex center to wall distance ($y_t = 0.05$ m).

The vortex center to wall distance y_t should be large enough to keep the vortex core sufficiently far from the boundary layer region to avoid overlapping of vortex vorticity distribution and the boundary layer vorticity distribution at initial time.

The solution of the vortex wall interaction in potential theory by Pellerin [8] helps us to define the interaction strength parameter:

$$\gamma = \frac{\Gamma}{4\pi U_\infty y_t}$$

In the following sections, we will present mostly results with $\gamma = -0.1$ and some with $\gamma = 0.1$.

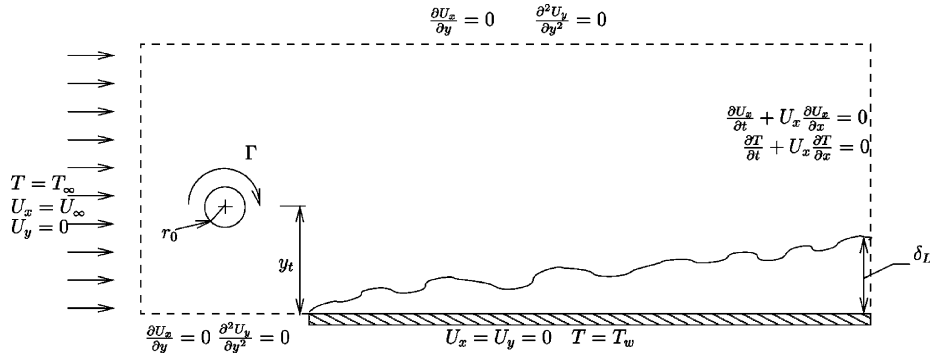

Fig. 5. Vortex boundary layer interaction: geometrical and numerical model.

5.2. Analysis of instantaneous field at $t = 0.1$

In order to clarify the different flow and temperature patterns, we analyse a snapshot of the flow during the interaction between the vortex and the boundary layer.

In Fig. 6, isovorticities and isotherms are reported in a magnified region near the wall under the vortex core center. The arrow indicates the station of the vortex center ($x_t = 0.542$ m). The important feature is the thinning of the boundary layer under the vortex after the vortex sweeping followed by thickening of the boundary layer ahead of the vortex station. Indeed, because of incompressibility, when the vortex's circulation is negative the longitudinal velocity gradient is negative just ahead of the vortex, leading to a increase of the transversal velocity and the boundary thickness.

The same phenomenon occurs for a vortex with positive sign of the circulation. However the effects are reversed, the thickening of the boundary layer being now after the vortex position. Indeed, the negative longitudinal velocity gradient is located downstream of the vortex station and leads to a increase of the boundary layer thickness right after the vortex position. Fig. 7 illustrates this fact showing the vorticity and temperature isolines underneath the vortex center at the position $x_t = 0.604$ m.

In Fig. 8, the variations of the boundary layer thicknesses for the negative vortex interaction are nor-

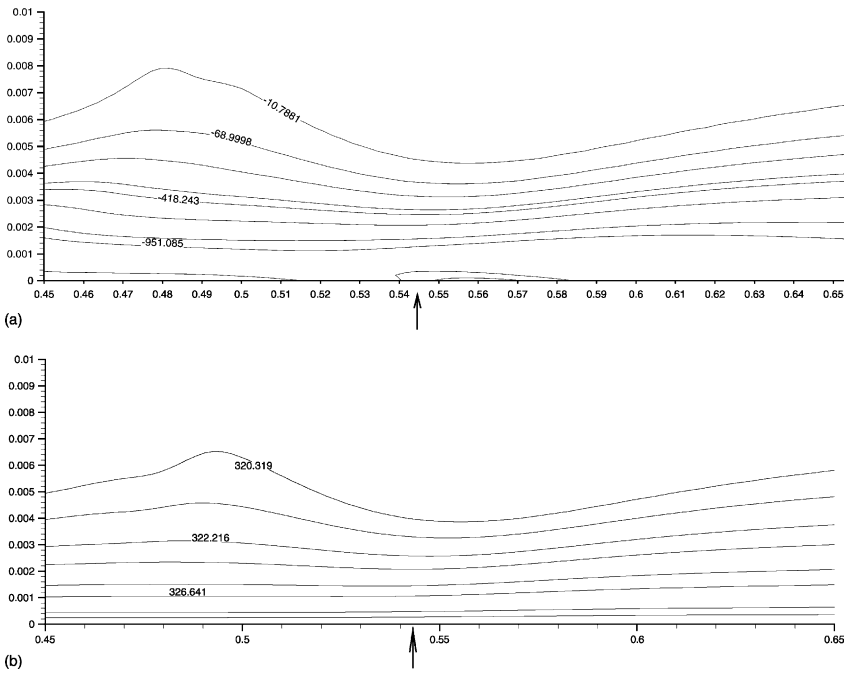

Fig. 6. (a) Vorticity field beneath the vortex. (b) Temperature field underneath the vortex, for $\gamma = -0.1$ at $t = 0.1$ s. The arrow indicates the position of the vortex center.

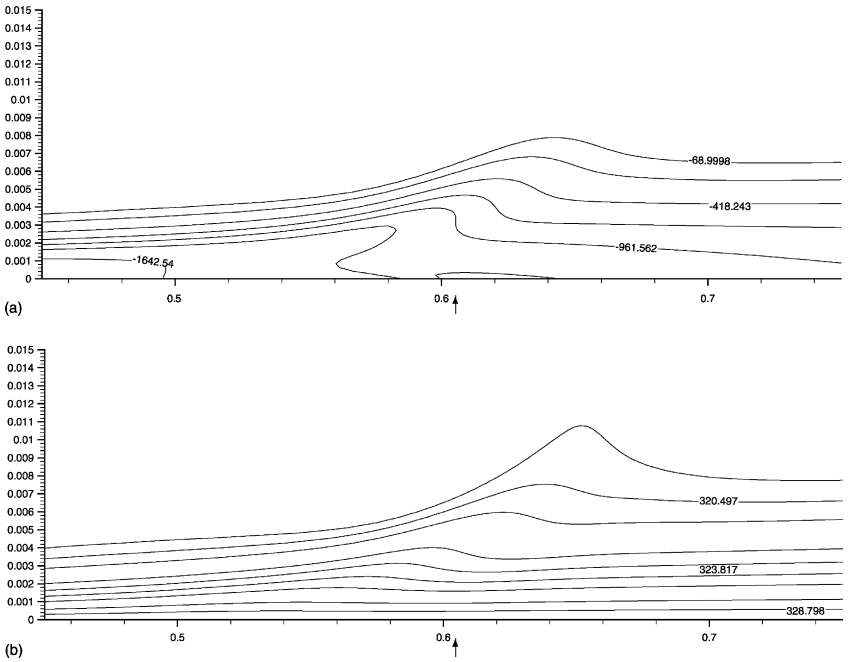

Fig. 7. (a) Vorticity field underneath the vortex. (b) Temperature field underneath the vortex, for $\gamma = 0.1$ at $t = 0.1$ s. The arrow indicates the position of the vortex center.

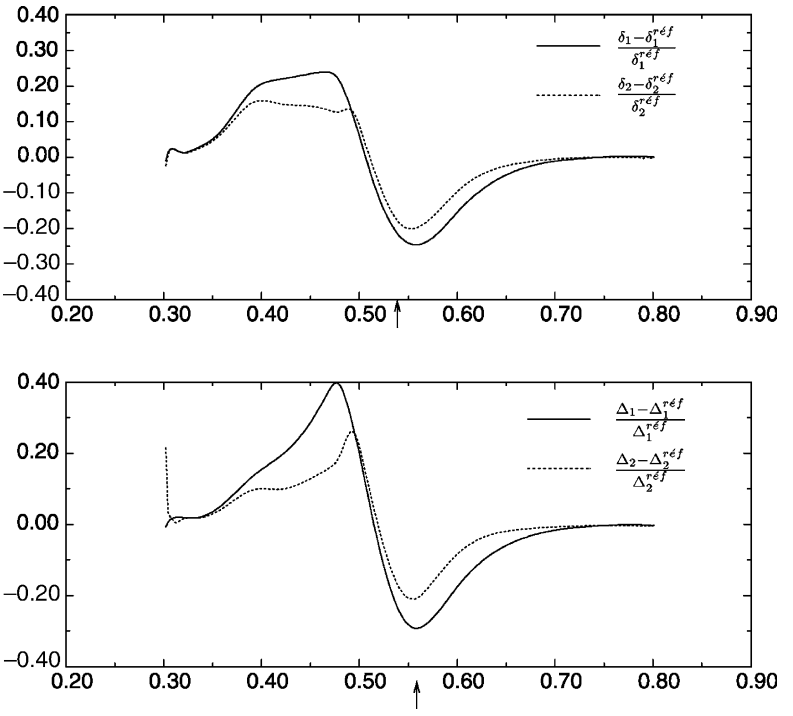

Fig. 8. Variations of the boundary layer thicknesses around reference values for $\gamma = -0.1$ at $t = 0.1$ s.

malized by the values of the flat plate boundary layer thicknesses.

In Fig. 9 are reported, for the negative vortex interaction, the values of the skin friction and the heat

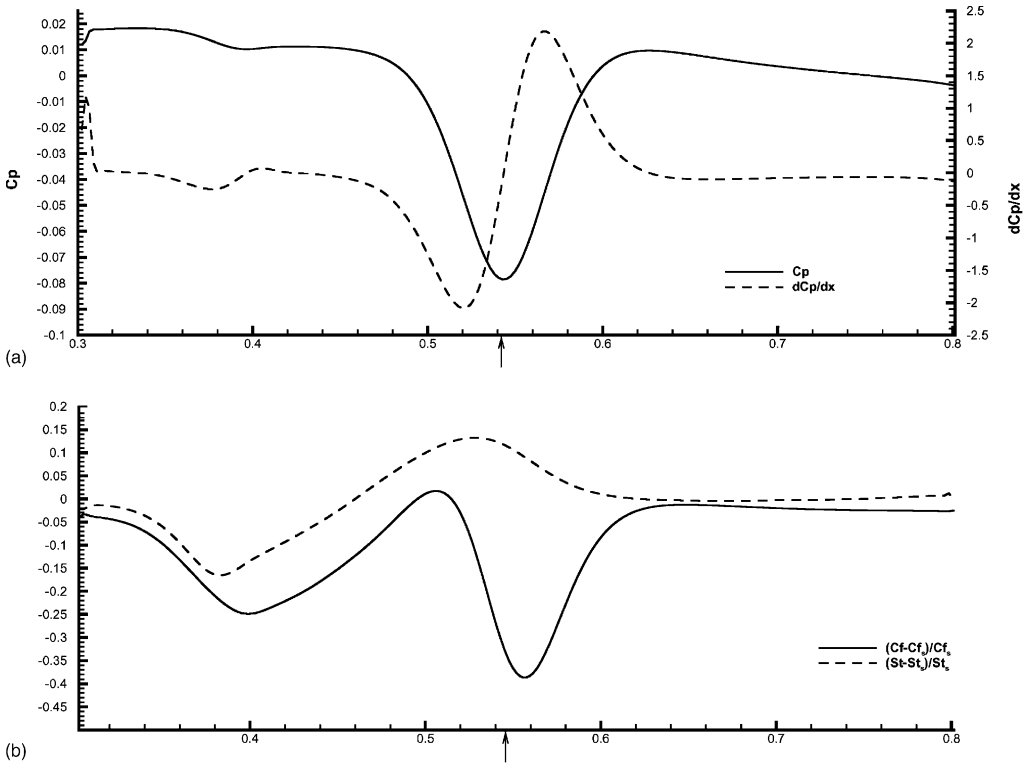

Fig. 9. Wall distributions at $t = 0.1$ s ($\gamma = -0.1$) of: (a) Pressure coefficient $Cp(x)$ and its derivative $(\mathrm{d}Cp/\mathrm{d}x)(x)$. (b) Normalized skin friction and heat transfer.

transfer coefficient relative to the steady flow values. We define the normalized skin friction and heat transfer coefficients as follows:

$$\overline{C}f = \frac{Cf - Cf_o}{Cf_o} \quad \overline{C}h = \frac{Ch - Ch_o}{Ch_o}$$

where Cf_o and Ch_o are respectively the flat plate skin friction and heat transfer coefficients. In the same figure, we plot the variations with respect to x of the pressure coefficient $Cp(x)$ and its first derivative $(\mathrm{d}C_p/\mathrm{d}x)(x)$. As reported in [8], we notice that the variation of the pressure minimum, $Cp_{\min}$, is a square function of γ and the position of this minimum is related to the vortex center position x_t ($Cp_{\min} = -\gamma^2/2$ in [8]). We notice too that the skin friction coefficient variation is similar to the one obtained through the pressure gradient term. Moreover, the inflexion point for the skin friction coefficient is very close to the vortex center x_t and the heat transfer coefficient exhibits a maximum beneath the vortex center.

5.3. Von Karman analysis

By application of von Karman analysis as described in Section 1, we split wall shear stress τ_w and wall heat flux φ_w as we stated in Table 1. Although slight modifications have been made in the rewriting of the external gradient term to enlighten the effect of the external pressure gradient. With hypothesis $\mathscr{H}_3$ and the above remark, the modified unsteady von Karman equations read as follows:

$$\frac{\tau_w}{\rho_\infty} = U_\infty \frac{\partial}{\partial t}(\delta_1) + \frac{\partial}{\partial x}(U_\infty^2 \delta_2) - \delta_1 \frac{\partial p_\infty}{\partial x} \tag{30}$$

$$\frac{\varphi_w}{\rho_\infty C_p (T_w - T_\infty)} = \frac{\partial \Delta_1}{\partial t} + \frac{\partial}{\partial x}(U_\infty \Delta_2) \tag{31}$$

Generically, for the skin friction equation the three terms are named respectively unsteady term, flat plate term and pressure gradient term. For the heat transfer, we have a unsteady term and a flat plate term. Each of the five terms have been evaluated with time and space differentiation of the unsteady velocity, pressure and temperature fields.

5.3.1. Negative circulation case: $\gamma = -0.1$

We illustrate in Fig. 10 each of these terms at $t = 0.1$ s. We shall now make the following observations:

With respect to the dynamic terms: the unsteady contribution reaches a maximum downstream with respect to the vortex center position and a minimum upward. Its amplitude under the vortex fingerprint of

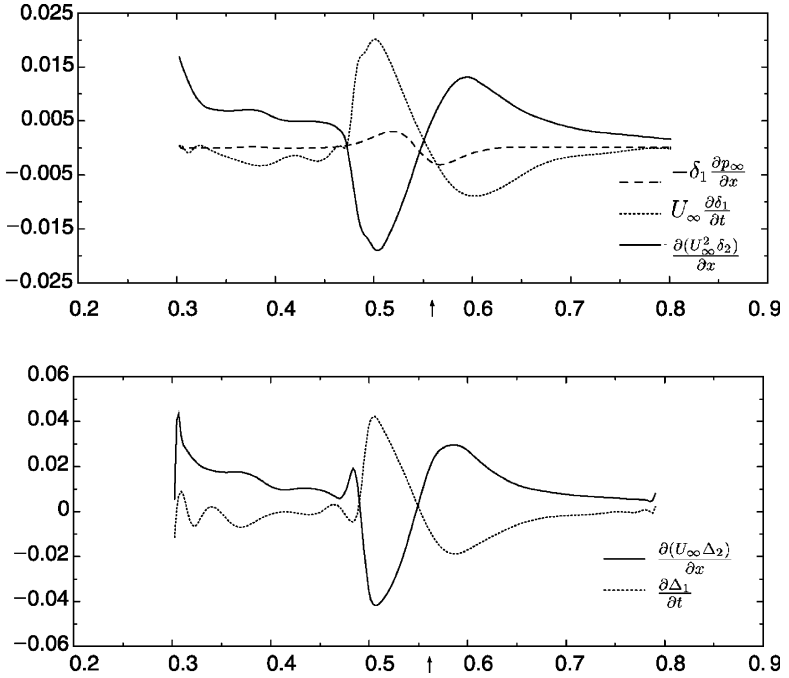

Fig. 10. Von Karman term decomposition: $\gamma = -0.1$ at $t = 0.1$ s. The arrow indicates the position x_t of the vortex center.

extension $2y_t$ is varying inversely with respect to the flat plate term. Besides, the third term, the external pressure gradient term contributes significantly to the variation of the wall shear stress along the plate.

With respect to the thermal terms: the unsteady term related with the displacement thickness and the flat plate term related with the enthalpy thickness are competing with one another. The remaining wall heat flux is the result of this competition. Underneath the vortex zone, the terms are qualitatively unsymmetrical, as in the dynamic case, but the sum ought to be strictly positive: wall heat flux keeps always positive values. Any explicit evidence tells us that the pressure gradient term is linked with the thermal equilibrium process in the boundary layer.

Finally, we report in Fig. 11, the evolution of the analogy factor at different snapshot times. The factor s is normalized by the non-interacting case value $Pr^{2/3}$. The abscissa is related to the moving frame coordinate travelling with vortex and normalized by the distance to the wall y_t. It is worth noting the rapidly growing value of the analogy factor peak underneath the vortex position with respect to the time. This evolution is confirmed with stronger interactions, i.e. stronger pressure gradient, where the peak value at a given time grows like γ^2.

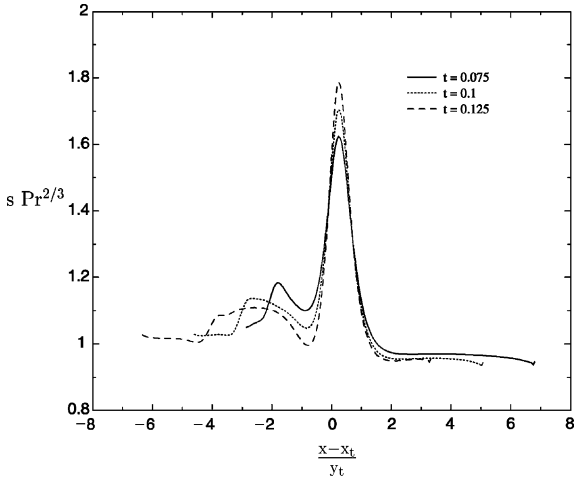

Fig. 11. Wall distribution of the unsteady analogy factor for $\gamma = -0.1$ in the vortex reference frame.

5.3.2. Positive circulation case: $\gamma = 0.1$

To give more insights on the analogy factor behavior, the positive circulation case ($\gamma = 0.1$) is shown in Fig. 12.

The analogy factor peak grows in the same manner as the negative vortex case. The main difference lies in the way the transfer coefficients are relaxing just after the vortex sweeping ($-4 < (x - x_t)/y_t < -0.5$). For negative vortex interactions, the analogy factor is greater than the reference state ($s = 1$) in this region. Whereas for positive vortex interaction, the different relaxation behavior of the boundary layer induces lower values than the

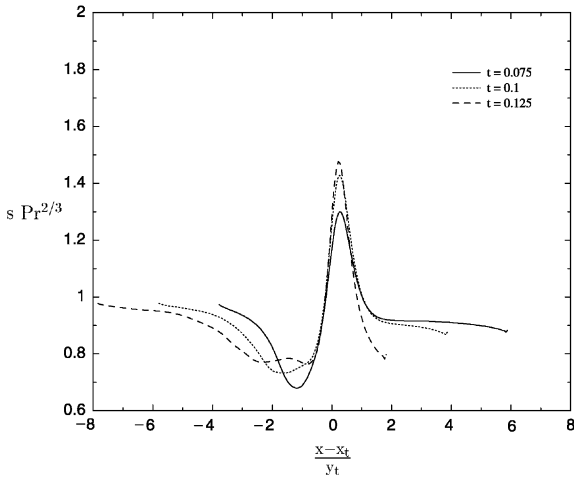

Fig. 12. Wall distribution of the unsteady analogy factor for $\gamma = 0.1$ in the vortex reference frame.

reference case for the analogy factor. For other interaction parameter values, we refer to [13].

6. Concluding remarks

In this paper we intend to put in evidence through von Karman integral budget method, the separated effects of unsteadiness and velocity or temperature gradients on momentum and heat flux wall transfer. We have shown the sensitivity of each of these terms against the physical properties of the fluid (Prandtl number) and flow characteristics (Eckert number, unsteadiness and pressure gradient).

The sensitivity to the pressure gradient is strong, nonlinear and prone to non-analogous boundary layer effects, this should be considered as the key argument for the analogy breakup. The Prandtl number is also obviously an influent parameter in the investigated range from 0.1 to 10.

In the second part of this paper, we evaluate separately the terms involved in the von Karman budget by numerical data post-processing. The simulated configuration focuses on the interaction of a transverse vortex with a flat plate boundary layer. The main remarks on this topic are the following:

The space and time dependent external pressure gradient plays a key role in the friction factor evolution. The heat flux peak under the vortex is related to the unsteady term.

Concerning the influence of the vortex circulation's sign on the analogy factor, we notice that in both cases the maximum is reached just under the vortex position. However a different behavior in the relaxation process of the boundary layer right after the vortex sweeping leads to greater values of the analogy factor compared to the reference case for the negative vortex and lower values for positive vortex.

More detailed parametric studies are in progress in order to investigate interactions with other values of the γ parameter and the effect of the Prandtl number variation. The final objective is the inclusion of these results into a database for thermal and dynamic turbulence modeling.

References

[1] W.M. Kays, M.E. Crawford, Convective Heat and Mass Transfer, third ed., McGraw-Hill, 1993.
[2] V.S. Arpaci, P.S. Larsen, Convection Heat Transfer, Prentice-Hall, 1984.
[3] J.K. Harvey, F.J. Perry, Flowfield produced by trailing vortices in the vicinity of the ground, AIAA J. 9 (8) (1971) 1659–1660.
[4] T.L. Doligalski, J.D.A Walker, Boundary layer induced by a convected two-dimensional vortex, J. Fluid Mech. 139 (1984) 1–28.
[5] J. Peube, B. Ferret, Réalisation et caractérisation d'un tourbillon reproductible, destiné à étudier des phénomènes instationnaires dans un cadre bidimensionnel, La Recherche Aérospatiale 4 (1991) 23–36.
[6] P. Reulet, Caractérisation expérimentale des échanges thermiques instationnaires en aérodynamique perturbée, PhD thesis, ENSAE, France, 1997.
[7] A. Corjon, A. Poinsot, Behavior of wake vortices near ground, AIAA J. 35 (5) (1997) 849–855.
[8] S. Pellerin, Interaction d'une structure tourbillonnaire avec une couche limite de plaque plane: Analyse et caractérisation des phénomènes aérodynamiques, PhD thesis, Université Paul Sabatier, France, 1997.
[9] D. Tafti, Vorticity dynamics and scalar transport in separated and reattached flow on a blunt plate, Phys. Fluids 5 (1993) 1661–1673.
[10] Brun, Martinot-Lagarde, Mécanique des Fluides, Dunod.
[11] A. Bejan, Convective Heat Transfer, Wiley & Sons, 1995.
[12] R. Panton, Incompressible Flow, Wiley & Sons, 1984.
[13] X. Escriva, Etude dynamique et thermique des transferts pariétaux instationnaires, Application à l'interaction tourbillon couche limite, PhD thesis, Université Paul Sabatier, France, 1999.
[14] V.M. Falkner, S.W. Skan, Some approximate solutions of the boundary layer equations, Philos. Mag. 12 (1931) 865–896.
[15] C.A. Schuler, E.B. Treidler, J.A.C. Humphrey, Cuteflows: An User Guide, Berkeley University, 1991.
[16] E.B. Treidler, A experimental and numerical investigation of flow past ribs in a channel, PhD thesis, University of California at Berkeley, United States of America, 1991.
[17] M.V. Bortolus, Modélisation et simulation des transferts thermiques pariétaux en écoulement turbulent com-

plexe, PhD thesis, Université Paul Sabatier, France, 1995.
[18] A. Giovannini, M.V. Bortolus, Transfert de chaleur au voisinage du point de recollement en aval d'une marche descendante, Revue Générale de Thermique 37 (1997) 89–107.
[19] H. Suzuki, J.A.C Humphrey, Flow past large obstructions between corotating disks in fixed cylindrical enclosures, ASME J. Fluids Eng. 119 (1997) 499–505.
[20] M.P. Dainese, Simulation numérique de l'écoulement de conduite à l'aval d'une conduite hélicoidale, in Congrès Français de Mécanique A.U.M, Poitiers, 1997.